Phosphatases modified by LH signaling in rat ovarian follicles and their role in regulating the NPR2 guanylyl cyclase

Jeremy R. Egbert[1#*], Ivan Silbern[2,3#], Tracy F. Uliasz[1], Katie M. Lowther[1,4], Siu-Pok Yee[1,4], Henning Urlaub[2,3*], and Laurinda A. Jaffe[1*]

[1]Department of Cell Biology, University of Connecticut Health Center, Farmington CT 06030 USA

[2]Bioanalytical Mass Spectrometry Group, Max Planck Institute for Multidisciplinary Sciences, 37077 Goettingen, Germany

[3]Institute of Clinical Chemistry, University Medical Center Goettingen, 37075 Goettingen, Germany

[4]Center for Mouse Genome Modification, University of Connecticut Health Center, Farmington CT 06030 USA

[#]These authors contributed equally to this paper.

*__Correspondence__: Department of Cell Biology, University of Connecticut Health Center, 263 Farmington Ave., Farmington, CT 06030 USA. Email: egbert@uchc.edu; henning.urlaub@mpinat.mpg.de; ljaffe@uchc.edu.

Running title: Phosphatase modifications in response to LH

Summary sentence: Mass spectrometric analysis of phosphatases whose phosphorylation state is rapidly modified by luteinizing hormone provides clues about how LH signaling dephosphorylates NPR2 as well as a resource for future studies.

Keywords: luteinizing hormone, ovary, phosphatase, phosphoproteomics, natriuretic peptide receptor

Abbreviations: bRP(basic reverse-phase), LH (luteinizing hormone), MS (mass spectrometry), NPR2 (natriuretic peptide receptor 2), PPP (phosphoprotein phosphatase), TMT (tandem mass tag)

Grant Support: This work was supported by the *Eunice Kennedy Shriver* National Institute of Child Health and Human Development (R37 HD014939 to L.A.J.), by the Fund for Science (600727 to L.A.J.), and by the University of Connecticut Health Center Research Advisory Council (to S.P.Y.). H.U. is funded by the Deutsche Forschungsgemeinschaft through collaborative research center SFB1286.

Abstract

In response to luteinizing hormone, multiple proteins in rat and mouse granulosa cells are rapidly dephosphorylated, but the responsible phosphatases remain to be identified. Because the phosphorylation state of phosphatases can regulate their interaction with substrates, we searched for phosphatases that might function in LH signaling by using quantitative phosphomass spectrometry. We identified all proteins in rat ovarian follicles whose phosphorylation state changed detectably in response to a 30-minute exposure to LH, and within this list, identified protein phosphatases or phosphatase regulatory subunits that showed changes in phosphorylation. Phosphatases in the PPP family were of particular interest because of their requirement for dephosphorylating the natriuretic peptide receptor 2 (NPR2) guanylyl cyclase, which triggers oocyte meiotic resumption. Among the PPP family regulatory subunits, PPP1R12A and PPP2R5D showed the largest increases in phosphorylation, with 4-10 fold increases in signal intensity on several sites. Although follicles from mice in which these phosphorylations were prevented by serine-to-alanine mutations in either *Ppp1r12a* or *Ppp2r5d* showed normal LH-induced NPR2 dephosphorylation, these regulatory subunits and others could act redundantly to dephosphorylate NPR2. Our identification of phosphatases and other proteins whose phosphorylation state is rapidly modified by LH provides clues about multiple signaling pathways in ovarian follicles.

Graphical Abstract

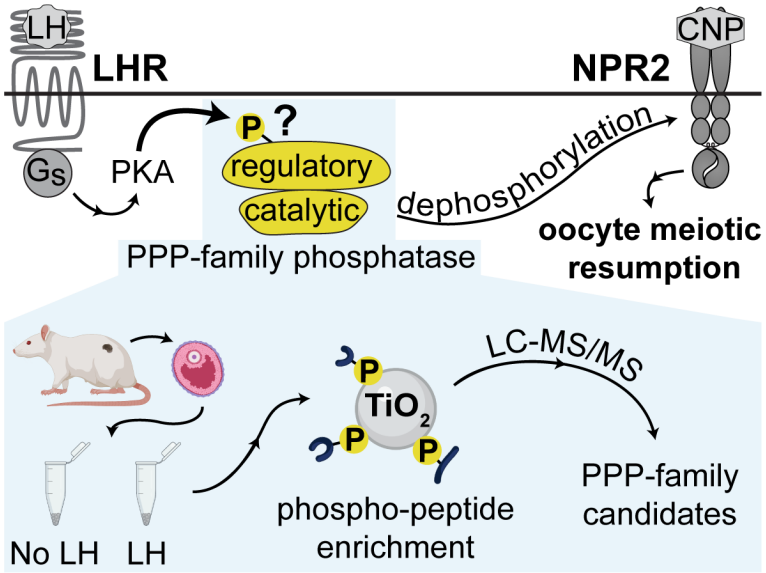

Introduction

Luteinizing hormone (LH) acts through its receptor in the mural granulosa cells of mammalian preovulatory follicles to activate G_s as well as other G-proteins, reinitiating meiosis and triggering ovulation (1-4). While much is known about protein kinase A and other kinases that are activated by LH/G_s signaling, little is known about which phosphatases are responsible for protein dephosphorylations that occur in response to the initial LH signal. Because phosphorylation of phosphatases can regulate their interaction with substrates (5-8), we searched for phosphatases that might function in LH signaling by using quantitative phospho-mass spectrometry.

Among the LH-induced events in the ovary that require phosphatase activity, oocyte meiosis is triggered to resume by a process that depends on the dephosphorylation and inactivation of the natriuretic peptide receptor (NPR2) guanylyl cyclase in the mural granulosa cells of the follicle (9-12). If dephosphorylation of NPR2 is prevented by changing its juxtamembrane serines and threonines to the phosphomimetic glutamate, meiotic resumption is delayed by several hours (11). The LH-induced dephosphorylation of NPR2 is prevented by small molecule inhibitors of PPP family phosphatases, cantharidin and okadaic acid (9), but the particular phosphatase holoenzymes that are responsible for the dephosphorylation and inactivation of NPR2 or other related guanylyl cyclases are unknown (13).

Each PPP family phosphatase holoenzyme is comprised of a catalytic subunit belonging to 1 of 7 subfamilies (PPP1c-PPP7c), in complex with 1 or 2 other subunits. Over 250 proteins are known to form complexes with PPP phosphatase catalytic subunits (14, 15), and these have been characterized with varying degrees of certainty to be regulators of PPP family phosphatase activity. ~60 of the best characterized are given names including “PPP” (14, 15). We used our phospho-mass spectrometric data to obtain clues about which among this large

number of candidates might regulate NPR2 dephosphorylation and other responses to LH signaling in ovarian follicles.

Materials and Methods

Animals

Rats (CD-Sprague-Dawley, Charles River Laboratories, Kingston, NY) and mice (C57BL/6J, Jackson Laboratory, Bar Harbor, ME) were used for these studies. Where indicated, mice were genetically modified using CRISPR-Cas9 to insert a hemagglutinin (HA) tag on *Npr2* (16), or to insert point mutations in *Ppp1r12a* (S507A, Figure S1) or *Ppp2r5d* (S53A/S81A/S82A/S566A, Figure S2). Mice with these mutations in phosphatase regulatory subunits also had an HA tag on *Npr2*. All procedures were approved by the animal care committee of the University of Connecticut Health Center. The genetically modified mice described here are available from Siu-Pok Yee upon request (syee@uchc.edu). The HA-*Npr2* mice are also available from the MMRRC Repository (MMRRC #71304; C57BL/6J-*Npr2*^{em1Laj}/Mmjax; JR#038421).

Ovarian follicles: isolation, culture and sample preparation

Preovulatory rat follicles, 700 - 900 μm in diameter, were dissected from the ovaries of 25-day old prepubertal animals that had been injected 48 hours previously with equine chorionic gonadotropin (National Hormone and Peptide Program, 12 I.U.) to stimulate follicle growth and LH receptor expression (9). The follicles were cultured for 1-2 hours on 30 mm Millicell cell culture inserts (PICMORG50, MilliporeSigma, St. Louis, MO) as previously described (9). LH (ovine LH-26, National Hormone and Peptide Program) was applied to the medium under the culture membrane, and a small drop was also added to the top of the membrane around each follicle, to ensure rapid exposure of the follicles. LH was used at 350 nM (10 μg/ml), a concentration that results in a maximal percentage of nuclear envelope breakdown in rat follicles under the conditions used here (17), and maximal dephosphorylation of NPR2 at 30 min (9). At 30 min after applying LH or control vehicle (PBS), follicles were washed in PBS, then frozen in liquid nitrogen and stored at -80°C, for mass spectrometry. Each rat follicle contains

~20 μg of protein as determined by a BCA assay (17), and 17-27 follicles were obtained per rat. Each sample for mass spectrometry contained 1.0-1.6 mg protein (50-81 follicles).

Fully grown mouse follicles, 300 - 400 μm in diameter, were dissected from the ovaries of 24-26 day old prepubertal animals that had not been injected with hormones. The follicles were then cultured for 23-26 hours on 30 mm Millicell cell culture inserts (PICMORG50), in the presence of 1 nM FSH (30 ng/ml, ovine FSH, National Hormone and Peptide Program) to stimulate synthesis of LH receptors and progression to the preovulatory stage (18). For some experiments, the FSH-cultured follicles were then incubated with or without the PPP phosphatase inhibitor cantharidin (C7632, Sigma-Aldrich) or the PKA inhibitor Rp-8-CPT-cAMPS (C011-05, BioLog, Bremen, Germany). LH or control vehicle (PBS) was then applied as described for rat follicles. LH was used at 10 nM (~0.3 μg/ml), the lowest concentration needed to achieve maximal nuclear envelope breakdown in mouse follicle-enclosed oocytes (18). For experiments with or without Rp-8-CPT-cAMPS, the volume required was minimized by transferring follicles to 12 mm Millicells (PICM01250) in a 4-well plate containing 250 μl medium. For western blotting, follicles that had been treated with or without LH for 30 minutes were washed in PBS, and then lysed by probe sonication in Laemmli sample buffer with 75 mM dithiothreitol and protease and phosphatase inhibitors as previously described (19). Each mouse follicle contains ~3.5 μg of protein as determined by a BCA assay (20).

Sample preparation for LC-MS/MS

For LC-MS/MS sample preparation (Figure 1), LC/MS-grade water, methanol, and acetonitrile (ACN) (Merck, Darmstadt, Germany) were used. Frozen rat ovarian follicles were homogenized in 400 μL lysis buffer (100 mM HEPES, pH 8, 4% SDS, 1mM EDTA, 1 × Halt protease/phosphatase inhibitor cocktail (ThermoFisher Scientific) using Zirconia/glass beads in a bead beating grinder (FastPrep24, MP Biomedicals). The lysates were sonicated in a

BioRuptor (Diagenode) for 5 min (30 s on/30 s off cycle). After clearing by centrifugation, protein concentration in the supernatant was determined using a BCA assay (ThermoFisher Scientific). Equal protein amounts were reduced/alkylated by incubating with 10 mM TCEP/ 40 mM CAA for 30 min at 37°C, and proteins were precipitated with methanol-chloroform (21). Precipitated proteins were resuspended in 1% RapiGest (Waters) in 100 mM TEAB, and digestion, phosphopeptide enrichment, isobaric TMT6 labeling, sample desalting, and basic-reversed phase (bRP) fractionation were performed as described previously (22). Aliquots of protein digests containing mostly non-phosphorylated peptides were separately labeled using TMT reagents processed within the same pipeline omitting the enrichment step. Two changes were made in the protocol: 1) Equal amounts of proteins were digested overnight using either trypsin (1:40 trypsin-to-protein ratio) or LysC (1:100 LysC-to-protein ratio), and then LysC- or trypsin-digested aliquots of the same sample were respectively combined before phosphopeptide enrichment. 2) Following bRP fractionation, 20 concatenated fractions were collected and analyzed.

LC-MS/MS

Dried bRP fractions of peptides prior to and after phosphopeptide enrichment were dissolved in 2% (v/v) ACN 0.1% (v/v) TFA in water and subjected to LC-MS/MS analysis using a setup as previously described (22, Figure 1). Phosphorylated peptides were injected in technical duplicates and separated using an 88 min gradient consisting of loading at 98% buffer A (0.1% (v/v) FA in water) 2% buffer B (80% ACN (v/v) 0.1% FA (v/v) in water) for 4 min; linear gradient ranging from 7% to 32% B over 56 min; followed by linear increase to 50% B over 18 min, washing step at 90% B for 5 min and re-equilibration step at 2% B for 5 min. For the separation of non-phosphorylated peptides, the first two steps were adjusted accordingly: 1) loading at 5% B for 5 min; 2) linear gradient from 8 to 34% B over 56 min.

An Orbitrap/Ion Trap mass spectrometer (Tribrid Fusion, ThermoFisher Scientific) was operated in data-dependent acquisition mode. Survey MS1 scans were acquired in Orbitrap at the resolution of 120,000, scan range 350-2000 *m/z,* normalized automatic gain control (AGC) target of 250%, and maximum injection time (maxIT) of 50 ms. The most abundant precursors of charge state 2-7 were subjected to fragmentation using HCD and normalized collision energy (NCE) of 33%. The length of the duty cycle was fixed to 3 s. Precursor ions were excluded from repetitive fragmentation for 30 s. MS2 spectra were acquired at the resolution of 30,000, normalized AGC target of 1000%, and 200 ms maxIT. The top 10 fragment ions were isolated using synchronous precursor selection (SPS; 23) and fragmented in HCD at NCE of 50%. Resulting SPS-MS3 spectra were acquired in Orbitrap at 50,000 resolution, normalized AGC target of 500% and maxIT of 200ms. When analyzing non-phosphorylated peptides, the resolution and maxIT of MS2 scans were reduced to 15,000 and 54 ms, respectively. Accordingly, maxIT of SPS-MS3 scans was set to 86 ms.

LC-MS/MS data analysis

Raw LC-MS/MS data were processed using MaxQuant software (version 1.6.2.10; 24) using default settings if not stated otherwise. MS-data from phosphorylated and non-phosphorylated peptides were processed simultaneously after defining “Phospho (S,T,Y)” modification as variable modification in the group parameters for the samples after the enrichment step. Other default modifications included carbamidomethylation of cysteine residues (fixed) and oxidation of methionine and acetylation of protein N-terms (both variable modifications). Up to five variable modifications were allowed per peptide. Trypsin was selected as protease. “Reporter ion MS3” was selected as quantification parameter. Default mass tolerances were preserved at 4.5 ppm and 20 ppm for precursor and fragment masses, respectively. Canonical protein sequences of *Rattus norvegicus* were downloaded from UniProt (February 2019, 29951 entries;

25). Further steps of statistical analysis were conducted in R programming language using custom scripts as previously described (22). In brief, impurity-corrected reporter ion intensities were used to assess differential abundance of phosphorylated peptides at the level of phosphorylation sites ("Phospho(S,T,Y).txt" output table of MaxQuant). Only phosphorylation sites with localization probability >0.75 were considered for the analysis. Reporter ion intensities were $\log_2$-transformed, normalized by median polishing, and subjected to differential expression testing using *limma* (26). *Limma*-moderated p-values were subjected to multiple testing corrections (27). Phosphorylation events were considered as significantly altered ("candidates") if satisfying the following criteria: 1) absolute $\log_2$ (Treated/Control) > $\log_2(1.5)$ and 2) *q*-value < 0.01. Impurity-corrected protein group intensities ("proteinGroups.txt" output table) were analyzed in a similar way in order to confirm that treatment had no significant impact on the proteome level.

Because of the similarity in amino acid sequences for PPP1R12A and R12B, peptides from these 2 proteins were indistinguishable. The assignment of these peptides to PPP1R12A was determined by ddPCR analysis of the relative abundances of PPP1R12A and R12B mRNAs (Figure S3).

Bioinformatics analysis

Lists of ovarian follicle proteins that had at least one site with one statistically significant difference in phosphorylation intensity following LH stimulation were subjected to gene set enrichment analysis using DAVID (2021 Update; 28). Gene ontology (GO) terms were considered significant if the Benjamini-Hochberg adjusted $p < 0.01$. Follicle GO terms with at least 5 gene products were downloaded March 18, 2022.

Western blotting

Proteins were separated by standard SDS-polyacrylamide gel electrophoresis (PAGE), or in a gel containing the phosphate binding molecule Phos-tag, as previously described (9, 29). Follicle lysates (20-60 μg protein) were directly loaded onto the gels without immunoprecipitation. Phos-tag reagent and compatible molecular weight markers were obtained from Fujifilm Wako Chemicals USA (Richmond, VA; cat. #AAL-107 and #230-02461, respectively). The antibodies used for western blotting are listed in Table S1.

To quantify changes in PPP1R12A phosphorylation in response to LH, we ran replicate lanes of the same lysates on a single gel and probed individual strips with antibodies to total or phosphorylated sites of PPP1R12A. To provide signal linearity, fluorescently labeled secondary antibodies were detected with an Odyssey imager (LI-COR, Lincoln, NE). LH-induced changes were calculated by first normalizing the phospho-PPP1R12A band intensity in the control or LH-treated lanes to those of the total PPP1R12A strip, and then normalizing to the control lane within each strip.

Statistics

Data were analyzed using Prism 9 (Graphpad Software, Boston, MA) as described in the figure legends.

Results and Discussion

Mass spectrometric analysis of LH-induced changes in the phosphoproteome of rat ovarian follicles

Using a mass spectrometry (MS)-based quantification strategy relying on tandem mass tag (TMT) labelling (22) (Figure 1), we first analyzed all proteins in rat ovarian follicles that showed detectable changes in phosphorylation in response to LH. Isolated preovulatory ovarian follicles were treated with or without LH for 30 min, then lysates were prepared for TMT-based quantitative MS; rats rather than mice were used in order to obtain sufficient protein.

Proteins extracted from LH-stimulated and non-stimulated ovarian follicles were digested with endoproteinase and enriched for phosphopeptides in parallel; the phosphopeptides were then labeled with isotopically labeled TMT6 reagents. Peptides were pooled, prefractionated by basic reverse-phase chromatography (bRP), and finally analyzed by LC-MS/MS (Figure 1) (22). Our analysis identified 4097 phosphorylated proteins in ovarian follicles, of which 866 proteins had at least one site with a statistically significant difference in phosphorylation intensity following LH stimulation (Supplementary data files S1-S3). Many but not all previously described LH-induced protein phosphorylation changes were identified by this analysis. The absence of some known phosphorylation sites could result because particular peptides were degraded by the proteases used in generating the samples used for MS, or were not recovered during the initial fraction steps (30).

Many of the phosphorylation changes identified by our mass spectrometric analysis have not been previously described following LH stimulation, providing a new resource for future studies. Gene ontology analysis of the proteins showing significant changes in phosphorylation is included in Supplementary data files S4-S6. One clear outcome of this analysis was the robust and rapid effects of LH signaling on the cytoskeleton of follicle cells, likely primarily represented

by granulosa cells. For instance, half of the 21 significant GO “Biological Process” terms are directly related to the cytoskeleton and its reorganization (Supplementary data file 4). Similarly, among the 10 most significant GO “Cellular Compartment” terms, 5 are related to aspects of the cytoskeleton or motile processes (Supplementary data file 5). Additionally, many of the significant GO “Molecular Function” terms reflect binding to elements of the cytoskeleton, as well as binding to, or activity of, cytoskeletal regulators (Supplementary data file 6). Another topic on which our dataset may be illuminating is steroidogenesis. A recent study identifying proteins phosphorylated in response to cAMP elevation has provided clues for understanding of regulation of steroidogenesis in mouse Leydig cell tumor line (30). Our phosphoproteomic data revealed similar regulation of many of the same proteins and could provide insights into how LH rapidly stimulates steroid production in the follicle (31).

Strikingly, our results identified 347 proteins with sites that showed significant *decreases* in phosphorylation intensity in response to LH stimulation. Though inhibitory phosphorylations of some kinases could explain some of these changes, this finding suggests that protein kinase A signaling massively and rapidly increases phosphatase activity targeting multiple substrates. Identification of such phosphatases could contribute to understanding of multiple aspects of LH signaling.

Mass spectrometric analysis of LH-induced changes in phosphorylation of PPP family phosphatase regulatory subunits in rat ovarian follicles

Phosphatases in the PPP family are estimated to be responsible for ~90% of dephosphorylation events in eukaryotic cells (32), and are of particular interest because their activity is required for LH-stimulated meiotic resumption in oocytes in rat and mouse ovarian follicles, based on inhibition by cantharidin and okadaic acid (9; Figure 2A,B). None of the PPP family phosphatase catalytic subunits showed changes in phosphorylation in response to LH

(Supplementary data file S1). However, among the ~60 interacting proteins that have been best characterized as regulatory subunits of PPP family phosphatases, as indicated by their assignment of official names including "PPP" (14, 15), 6 showed statistically significant changes in phosphorylation in response to LH (Table 1). The 2 largest phosphorylation increases were in PPP2R5D (also known as PP2A-B56δ) and PPP1R12A (also known as MYPT1) (Table 1, Figure S3). Among the over 200 other proteins that are known to interact with PPP family phosphatase catalytic subunits (with non-"PPP" gene names), those that showed changes in phosphorylation in response to LH are listed in Table S2.

PPP2R5D showed an ~10x increase in phosphorylation signal intensity on serine 53, and a 4x increase on serine 566. PPP2R5D-S566 phosphorylation in response to LH receptor stimulation in rat ovarian granulosa cells has been reported previously (33), and phosphorylation of serine 566 is critical for activation of PPP2 by PKA in other cells (5). A marginally significant increase in phosphorylation intensity on serine 81 and serine 82 of PPP2R5D was also detected. PPP1R12A showed an ~4x increase in the signal intensity of phosphorylation of on serine 507, known to be a regulatory site in other cells (8). Another PPP1 regulatory subunit, PPP1R14A (also known as CPI-17), showed a 3-7 X *decrease* in phosphorylation signal intensity on serines 16 and 26 (Table 1).

These LH-dependent changes in phosphorylation of PPP family phosphatase regulatory subunits identified candidates for phosphatase complexes that might mediate dephosphorylation of NPR2 in response to LH signaling. Because LH-induced NPR2 dephosphorylation depends on the activation of protein kinase A, as demonstrated by inhibition by the PKA-specific inhibitor Rp-8-CPT-cAMPS (34) (Figure 2C-F), we focused on investigating regulatory subunits whose phosphorylation increased rather than decreased in response to LH.

Western blot confirmation of PPP1R12A and PPP2R5D phosphorylation increases in LH-treated mouse ovarian follicles

Consistent with the MS analysis, quantitative western blotting of mouse ovarian follicles using a phosphospecific antibody showed that LH caused an 11x increase in phosphorylation of PPP1R12A on serine 507 (Figure 3A,B). A 3x increase in phosphorylation on serine 668 was also detected (Figure 3A,B), as previously seen with LH receptor stimulation of granulosa cells from rat preovulatory follicles (35). 3 other sites on PPP1R12A showed no change in phosphorylation in response to LH (Figure 3A,B). Inhibition of serine 507 phosphorylation by the PKA-specific inhibitor Rp-8-CPT-cAMPS (34) showed that the LH response depended on protein kinase A (Figure 3C,D), like the LH-induced dephosphorylation of NPR2 (Figure 2C,D).

Phosphospecific antibodies were not available for PPP2R5D, so as an alternative, we used Phos-tag gel electrophoresis (36) followed by western blotting with antibodies against the total proteins. Using this approach, we confirmed that LH increased phosphorylation of PPP2R5D in mouse ovarian follicles, and determined that the phosphorylation was PKA-dependent (Figure 4A,B).

Investigation of the function of LH-induced phosphorylation of PPP family phosphatase regulatory subunits in pathways leading to NPR2 dephosphorylation, using genetically modified mice with serine-to-alanine mutations

Our MS and western blotting results suggested PKA-dependent phosphorylation of PPP1R12A on serine 507, and of PPP2R5D on serines 53 and 566, as possible mediators of LH-induced NPR2 dephosphorylation. Phosphorylations of these sites could potentially increase the interaction of the regulatory subunits with the NPR2 protein, bringing the associated catalytic subunits close to NPR2. The known substrate interaction motif for PPP2R5D, LxxIxE within an intrinsically disordered region (32), is not found in NPR2, and although PPP1R12A contains a

motif that binds its catalytic subunit, a general motif that serves to recruit PPP1R12A to substrates is thus far unknown (37). However, other as yet uncharacterized interaction sites could be present in the NPR2 protein that mediate either direct or indirect binding to PPP1R12A or PPP2R5D.

Due to the low abundance of NPR2 in follicles, and the limited amount of follicle protein that could be obtained, searching for such interaction sites by coimmunoprecipitation was not attempted. Instead, we tested the function of the phosphorylated sites by making serine-to-alanine substitutions, an approach that was used effectively to analyze phosphorylation changes detected in a previous mass spectrometry study (22). We generated 2 mouse lines in which the serines in PPP1R12A and PPP2R5D that were phosphorylated in response to LH were changed to alanines (Figures S1, S2), to test whether these LH-induced phosphorylations are required for NPR2 dephosphorylation. The mouse lines that we made with global serine-to-alanine modifications were viable and did not show obvious morphological or physiological defects. Homozygous mice were fertile, although fertility was not investigated quantitatively.

In the first of these mouse lines, in which serine 507 of *Ppp1r12a* was changed to alanine, western blots confirmed that ovarian follicles did not show the LH-induced increase in PPP1R12A-S507 phosphorylation that was seen in wildtype follicles (Figure 5A). We then investigated whether the S507A mutation inhibited the LH-stimulated dephosphorylation of NPR2, and found that it did not (Figure 5B,C).

In a second mouse line, serines 53 and 566 of *Ppp2r5d* were changed to alanines, corresponding to the 2 sites that showed significantly increased phosphorylation in response to LH (Table 1). Because the peptide containing serines 81 and 82 also showed increases in phosphorylation intensity that approached significance (Table 1), these sites were also changed to alanines. The resulting mouse line with the 4 serine-to-alanine mutations was called *Ppp2r5d*-S53A/S81A/S82A/S566A or *Ppp2r5d*-4A for short. Phostag gel electrophoresis of protein in

follicles from mice with these 4 mutations showed much reduced basal phosphorylation of the PPP2R5D protein, and no increase in phosphorylation in response to LH (Figure 6A). However, as with the *Ppp1r12a*-S507A mice, the *Ppp2r5d*-4A mice showed no inhibition of LH-induced dephosphorylation of NPR2 (Figure 6B,C). These results indicated that neither of these individual regulatory subunits of PPP1 and PPP2 is by itself responsible for LH-induced dephosphorylation of NPR2.

Whether mice with these mutations in *both Ppp1r12a* and *Ppp2r5d* would show inhibition of LH-induced dephosphorylation of NPR2 will be useful to examine, as different PPP family proteins can have overlapping functions. In a recent study, mice lacking *Ppp2r5d* or *Ppp2r5c* had no overt phenotypes, but mice lacking both of these genes were arrested at embryonic day 12 due to a heart defect (38). LH also induced smaller (2-3 fold) but significant increases in phosphorylation signal intensity of serines in PPP2R5A, PPP1R9A, and PPP2R5C (Table 1), as well as significant increases in several other less well characterized PPP interacting proteins (Table S1), raising the possibility of even more complex redundancy. The large LH-induced *decrease* in phosphorylation of several sites of the R14A regulatory subunit of PPP1 (Table 1) suggests PPP1R14A as another possible regulator of LH-induced dephosphorylation of NPR2, although the decrease in R14A phosphorylation could not be a direct action of PKA.

Alternatively, LH signaling could cause NPR2 dephosphorylation by decreasing kinase activity, although the kinases responsible for phosphorylating the juxtamembrane serines of NPR2 are unknown (13). Stimulation of the LH receptor increases phosphorylation of glycogen synthase kinase β (GSK-β) on serine 9 (33) and this PKA-dependent phosphorylation inhibits GSK-β activity (39), suggesting a possible candidate. Our mass spectrometric analysis identified multiple serine/threonine kinases that are phosphorylated in response to LH

(Supplementary Data Files S1 and S3; see also related term in Supplementary Data File S6), suggesting other candidates that could be considered.

Identification of the PPP family phosphatases responsible for NPR2 dephosphorylation, or of kinases whose phosphorylation of NPR2 is decreased by LHR activation, will be useful not only for understanding of signaling in the ovary, but also in other systems in which the phosphorylation state of NPR2, or of the related guanylyl cyclase NPR1, controls function (13, 40). For example, FGF inhibition of bone growth depends at least in part on NPR2 dephosphorylation by a PPP family phosphatase (29, 41-43).

LH-induced changes in phosphorylation of *non*-PPP family protein phosphatases in rat ovarian follicles.

In addition to the PPP family phosphatases described above, LH caused large changes in phosphorylation intensity of multiple protein phosphatases outside of the PPP family (Table 2). These include the Slingshot protein phosphatase 1 (SSH1), for which LH causes an ~4x increase in phosphorylation intensity on serines 576 and 598 (Figure S4). SSH1 dephosphorylates and activates proteins in the cofilin/actin depolymerizing factor family (CFL1, CFL2, DSTN) (44), and is of high interest because LH signaling decreases cofilin phosphorylation in isolated granulosa cells, causing an increase in motility (45). Granulosa cell motility increases in intact ovarian follicles after the preovulatory surge of LH and may contribute to the ovulatory process (46).

Although it is unknown if the modifications of SSH1 on serines 576 and 598 increase its phosphatase activity, our MS screen revealed LH-induced decreases in phosphorylation intensity of the serine 3 regulatory sites of CFL1, CFL2, and DSTN to ~10% of baseline (Figure S4). Dephosphorylation of serine 3 on these proteins increases their activity (44). The LH-

induced phosphorylation of serines 576 and 598 of SSH1 suggests that LH might dephosphorylate and activate cofilin family members by way of SSH1.

A database of LH-induced protein phosphorylation changes as a resource for future studies

LH signaling in the granulosa cells of ovarian follicles has been previously shown to cause rapid changes in phosphorylation of multiple proteins (33, 47, 48). In the present study, we characterized LH-induced phosphorylation changes in rat ovarian follicles systematically, using quantitative phosphomass spectrometry. We then used this dataset to identify protein phosphatases that are modified by LH signaling, and to investigate their function in dephosphorylating the NPR2 guanylyl cyclase, which triggers oocyte meiotic resumption (9).

Inhibitor studies have indicated that PPP-family phosphatase activity is also required for LH stimulation of synthesis of progesterone (49). In addition, phosphatases outside of the PPP family are modified by LH signaling. Thus, our identification of phosphatase proteins whose phosphorylation state is modified by LH (Tables 1,2, and S2) may provide clues about multiple signaling pathways in ovarian follicles. More generally, these data (Supplementary Data Files 1-6) will be broadly useful for future studies of the many aspects of LH signaling that are mediated by changes in protein phosphorylation.

Supplementary material

This article contains supplementary material (Figures S1-S4, Tables S1 and S2, Supplementary Data Files S1-S6).

Data availability

The mass spectrometry data have been deposited to the ProteomeXchange Consortium via the PRIDE (50) partner repository with the data set identifier PXD033878.

Author contributions

JRE, IS, HU, and LAJ designed the study. IS and HU carried out the mass spectrometry studies. JRE, TFU, and LAJ carried out the western blotting studies. KML and SPY generated the genetically modified mice. JRE, IS, SPY, HU, and LAJ analyzed the data and wrote the manuscript; all authors approved the manuscript.

Conflict of interest

The authors declare that no conflict of interest exists.

Acknowledgments

We thank Monika Raabe for assistance in the sample preparation for LC-MS/MS, and Deborah Kaback and Iris Nakashima for assistance in generating the genetically modified mice. We also thank Lincoln Potter, Rebecca Page, Corie Owen, Leia Shuhaibar, Rachael Norris, and Melina Schuh for helpful discussions. We dedicate this paper to the memory of Alexei Evsikov, who inspired our studies of the bioinformatics of reproduction.

References

1. Jaffe LA, Egbert JR. Regulation of mammalian oocyte meiosis by intercellular communication within the ovarian follicle. *Annu Rev Physiol* 2017*;* **79**:237-260.
2. Richards JS, Ascoli M. Endocrine, paracrine, and autocrine signaling pathways that regulate ovulation. *Trends Endocrinol Metab* 2018; **29**:313-325.
3. Sposini S, Hanyaloglu AC. Driving gonadotrophin hormone receptor signalling: the role of membrane trafficking. *Reproduction* 2018; **156**:R195–R208.
4. Johnson GP, Jonas KC. Mechanistic insight into how gonadotropin hormone receptor complexes direct signaling. *Biol Reprod* 2020; **102**:773-783.
5. Ahn J-H, McAvoy T, Rakhilin, SV, Nishi A, Greengard P, Nairn AC. Protein kinase A activates protein phosphatase 2A by phosphorylation of the B56δ subunit. *Proc Natl Acad Sci USA* 2007; **104**:2979-2984.
6. Yamashiro S, Yamakita Y, Totsukawa G, Goto H, Kaibuchi K, Ito M, Hartshorne DJ, Matsumura F. (2008) Myosin phosphatase-targeting subunit 1 regulates mitosis by antagonizing polo-like kinase 1. *Develop Cell* 2008; **14**:787-797.
7. Brautigan DL, Shenolikar S. Protein serine/threonine phosphatases: keys to unlocking regulators and substrates. *Ann Rev Biochem* 2018; **87**:921-964.
8. Samson SC, Elliott A, Mueller BD, Kim Y, Carney KR, Bergman JP, Blenis J, Mendoza MC. p90 ribosomal S6 kinase (RSK) phosphorylates myosin phosphatase and thereby controls edge dynamics during cell migration. *J Biol Chem* 2019; **294**:10846-10862.
9. Egbert JR, Shuhaibar LC, Edmund AB, Van Helden DA, Robinson JW, Uliasz TF, Baena V, Geerts A, Wunder F, Potter LR, Jaffe LA. Dephosphorylation and inactivation of the NPR2 guanylyl cyclase in the granulosa cells contributes to the LH-induced cGMP decrease that causes resumption of meiosis in rat oocytes. *Development* 2014; **141**:3594-3604.

10. Shuhaibar LC, Egbert JR, Norris RP, Lampe PD, Nikolaev VO, Thunemann M, Wen L, Feil R, Jaffe LA. Intercellular signaling via cyclic GMP diffusion through gap junctions in the mouse ovarian follicle. *Proc Natl Acad Sci USA* 2015; **112**:5527-5532.
11. Shuhaibar LC, Egbert JR, Edmund AB, Uliasz TF, Dickey DM, Yee S-P, Potter LR, Jaffe LA. Dephosphorylation of juxtamembrane serines and threonines of the NPR2 guanylyl cyclase is required for rapid resumption of oocyte meiosis in response to luteinizing hormone. *Dev Biol* 2016; **409**:194-201.
12. Egbert JR, Robinson JW, Uliasz TF, Potter LR, Jaffe LA. Cyclic AMP links luteinizing hormone signaling to dephosphorylation and inactivation of the NPR2 guanylyl cyclase in ovarian follicles. *Biol Reprod* 2021; **104**:939-941.
13. Potter LR. Phosphoregulation of membrane guanylyl cyclases: from chemical discovery to physiologic signaling. *J Biol Chem* 2023; (in press)
14. Bollen M, Peti W, Ragusa MJ, Beullens M. The extended PP1 toolkit: designed to create specificity. *Trends Biochem Sci* 2010; **35**:450-458.
15. Brauer BL, Wiredu K, Mitchell S, Moorhead GB, Gerber SA, Kettenbach AN. Affinity-based profiling of endogenous phosphoprotein phosphatases by mass spectrometry. *Nat Protoc* 2021; **16**:4919-4943.
16. Baena V, Owen CM, Uliasz TF, Lowther KM, Yee S-P, Terasaki M, Egbert JR, Jaffe LA. Cellular heterogeneity of the LH receptor and its significance for cyclic GMP signaling in mouse preovulatory follicles. *Endocrinology* 2020; **161**:bqaa074.
17. Egbert JR, Uliasz TF, Shuhaibar LC, Geerts A, Wunder F, Kleiman RJ, Humphrey JM, Lampe PD, Artemyev NO, Rybalkin SD, Beavo JA, Movsesian MA, Jaffe LA. Luteinizing hormone causes phosphorylation and activation of the cyclic GMP phosphodiesterase PDE5 in rat ovarian follicles, contributing, together with PDE1 activity, to the resumption of meiosis. *Biol Reprod* 2016; **94**(5):110.

18. Vigone G, Shuhaibar LC, Egbert JR, Uliasz TF, Movsesian MA, Jaffe LA. Multiple cAMP phosphodiesterases act together to prevent premature oocyte meiosis and ovulation. *Endocrinology* 2018; **159**:2142-2152.
19. Egbert JR, Yee S-P, Jaffe LA. Luteinizing hormone signaling phosphorylates and activates the cyclic GMP phosphodiesterase PDE5 in mouse ovarian follicles, contributing an additional component to the hormonally induced decrease in cyclic GMP that reinitiates meiosis. *Dev Biol* 2018; **435**:6-14.
20. Norris RP, Freudzon M, Mehlmann LM, Cowan AE, Simon AM, Paul DL, Lampe PD, Jaffe LA. Luteinizing hormone causes MAP kinase-dependent phosphorylation and closure of connexin 43 gap junctions in mouse ovarian follicles: one of two paths to meiotic resumption. *Development* 2008; **135**:3229-3238.
21. Wessel D, Fluegge UI. A method for the recovery of protein in dilute solution in the presence of detergents and lipids. *Anal Biochem* 1984; **138**:141-143.
22. Silbern I, Pan K-T, Fiosins M, Bonn S, Rizzoli SO, Fornasiero EF, Urlaub H, Jahn R. Protein phosphorylation in depolarized synaptosomes: dissecting primary effects of calcium from synaptic vesicle cycling. *Mol Cell Proteom* 2021; **20**:100061.
23. McAlister GC, Nusinow DP, Jedrychowski MP, Wühr M, Huttlin EL, Erickson BK, Rad R, Haas W, Gygi SP. MultiNotch MS3 enables accurate, sensitive, and multiplexed detection of differential expression across cancer cell proteomes. *Anal Chem* 2014; **86**:7150-7158.
24. Tyanova S, Temu T, Cox J. The MaxQuant computational platform for mass spectrometry-based shotgun approaches. *Nat Protoc* 2016; **11**:2301-2319.
25. UniProt Consortium. UniProt: a worldwide hub of protein knowledge. *Nucleic Acids Res* 2019; **47**:D506-D515.

26. Smyth GK. limma: Linear models for microarray data. 2005; In *Bioinformatics and Computational Biology Solutions Using R and Bioconductor*. R Gentleman, VJ Carey, W Huber, RA Irizarry, S Dudoit, (eds) Springer, New York, pp. 397-420.

27. Storey JD, Tibshirani R. Statistical significance for genomewide studies. *Proc Natl Acad Sci USA* 2003; **100**:9440-9445.

28. Sherman BT, Hao M, Qiu J, Jiao X, Baseler MW, Lane HC, Imamichi T, Chang W. DAVID: a web server for functional enrichment analysis and functional annotation of gene lists (2021 update). *Nucleic Acids Res* 2022; **50**:W216-W221.

29. Shuhaibar LC, Kaci N, Egbert JR, Horville T, Loisay L, Vigone G, Uliasz TF, Dambroise E, Swingle MR, Honkanen RE, Biosse Duplan M, Jaffe LA, Legeai-Mallet L. Phosphatase inhibition by LB-100 enhances BMN-111 stimulation of bone growth. *JCI Insight* 2021; **6**:e141426.

30. Beavo JA, Golkowski M, Shimizu-Albergine M, Beltejar M-C, Bornfeldt KE, Ong S-E. Phosphoproteomic analysis as an approach for understanding molecular mechanisms of cAMP-dependent actions. *Mol Pharmacol* 2021; **99**:342–357.

31. Light A, Hammes SR. LH-induced steroidogenesis in the mouse ovary, but not testis, requires matrix metalloproteinase 2- and 9-mediated cleavage of upregulated EGF receptor ligands. *Biol Reprod* 2015; **93**(3):65,1-13.

32. Wang X, Garvanska DH, Nasa I, Ueki Y, Zhang G, Kettenbach AN, Peti W, Nilsson J, Page R. A dynamic charge-charge interaction modulates PP2A:B56 substrate recruitment. *eLife* 2020; **9**:e55966.

33. Flynn MP, Maizels ET, Karlsson AB, McAvoy T, Ahn JH, Nairn AC, Hunzicker-Dunn M. Luteinizing hormone receptor activation in ovarian granulosa cells promotes protein kinase A-dependent dephosphorylation of microtubule-associated protein 2D. *Mol Endocrinol* 2008; **22**:1695-1710.

34. Schwede F, Maronde E, Genieser H-G, Jastorff B. Cyclic nucleotide analogs as biochemical tools and prospective drugs. *Pharmacol Ther* 2000; **87**:199-226.

35. Law NC, White MF, Hunzicker-Dunn ME. G protein-coupled receptors (GPCRs) that signal via protein kinase A (PKA) cross-talk at insulin receptor substrate 1 (IRS1) to activate the phosphatidylinositol 3-kinase (PI3K)/AKT pathway. *J Biol Chem* 2016; **291**:27160-27169.

36. Kinoshita E, Kinoshita-Kikuta E, Takiyama K, Koike T. Phosphate-binding tag, a new tool to visualize phosphorylated proteins. *Mol Cell Proteom* 2006; **5**:749-757.

37. Kiss A, Erdodi F, Lontay B. Myosin phosphatase: unexpected functions of a long-known enzyme. *BBA – Mol Cell Res* 2019; **1866**:2-15.

38. Dyson JJ, Abbasi F, Varadkar P, McCright B. Growth arrest of PPP2R5C and PPP2R5D double knockout mice indicates a genetic interaction and conserved function for these PP2A B subunits. *FASEB BioAdvances* 2022; **4**:273-282.

39. Fang X, Yu SX, Lu Y, Bast RC, Woodgett JR, Mills GB. Phosphorylation and inactivation of glycogen synthase kinase 3 by protein kinase A. *Proc Natl Acad Sci* 2000; **97**:11960-11965.

40. Egbert JR, Uliasz TF, Lowther KM, Kaback D, Wagner BM, Healy CL, O'Connell TD, Potter LR, Jaffe LA, Yee S-P. Epitope-tagged and phosphomimetic mouse models for investigating natriuretic peptide-stimulated receptor guanylyl cyclases. *Front Mol Neurosci* 2022; **15**:1007026.

41. Shuhaibar LC, Robinson JW, Vigone G, Shuhaibar NP, Egbert JR, Baena V, Uliasz TF, Kaback D, Yee S-P, Feil R, Fisher MC, Dealy CN, Potter LR, Jaffe LA. Dephosphorylation of the NPR2 guanylyl cyclase contributes to inhibition of bone growth by fibroblast growth factor. *eLife* 2017; **6**:e31343.

42. Robinson JW, Blixt NC, Norton A, Mansky KC, Ye Z, Aparicio C, Wagner BM, Benton AM, Warren GL, Khosla S, Gaddy D, Suva LJ, Potter LR. Male mice with elevated C-type

natriuretic peptide-dependent guanylyl cyclase-B activity have increased osteoblasts, bone mass and bone strength. *Bone* 2020; **135**:115320.

43. Wagner BM, Robinson JR, Lin Y-W, Li Y-C, Kaci N, Legeai-Mallet L, Potter LR. Prevention of guanylyl cyclase-B dephosphorylation rescues achondroplastic dwarfism. *JCI Insight* 2021; **6**:e147832.
44. Huang TY, DerMardirossian C, Bokoch GM. Cofilin phosphatases and regulation of actin dynamics. *Curr Opin Cell Biol* 2006; **18**:26-31.
45. Karlsson AB, Maizels ET, Flynn MP, Jones JC, Shelden EA, Bamburg JR, Hunzicker-Dunn M. Luteinizing hormone receptor-stimulated progesterone production by preovulatory granulosa cells requires protein kinase A-dependent activation/dephosphorylation of the actin dynamizing protein cofilin. *Mol Endocrinol* 2010; **24**:1765-1781.
46. Owen CM, Jaffe LA. Luteinizing hormone stimulates ingression of granulosa cells within the mouse preovulatory follicle. *BioRxiv* 2023; 04.21.537855; doi: https://doi.org/10.1101/2023.04.21.537855
47. Hunzicker-Dunn M, Mayo K. Gonadotrophin signaling in the ovary. In: TM Plant, AJ Zeleznik, eds. Knobil and Neill's Physiology of Reproduction. 4th ed. San Diego: Academic Press, 2015; pp. 895-945.
48. Flynn MP, Fiedler SE, Karlsson AB, Carr DW, Maizels ET, Hunzicker-Dunn M. Dephosphorylation of MAP2D enhances its binding to vimentin in preovulatory ovarian granulosa cells. *J Cell Science* 2016; **129**:2983-2996.
49. Yu C-C, Chen W-Y, Li PS. Protein phosphatase inhibitor cantharidin inhibits steroidogenesis and steroidogenic acute regulatory protein expression in cultured rat preovulatory follicles. *Life Sci* 2001; **70**:57-72.
50. Perez-Riverol Y, Csordas A, Bai J, Bernal-Llinares M, Hewapathirana S, Kundu DJ, Inuganti A, Griss J, Mayer G, Eisenacher M, Perez E, Uszkoreit J, Pfeuffer J, Sachsenberg T, Yilmaz

S, Tiwary S, Cox J, Audain E, Walzer M, Jarnuczak AF, Ternent T, Brazma A, Vizcaíno JA. The PRIDE database and related tools and resources in 2019: improving support for quantification data. *Nucleic Acids Res* 2019; **47**:D442-D450.

51. Swingle MR, Honkanen RE. Inhibitors of serine/threonine protein phosphatases: biochemical and structural studies provide insight for further development. *Curr Med Chem* 2019; **26**:2634-2660.
52. Sacco F, Perfetto L, Castagnoli L, Cesareni G. The human phosphatase interactome: An intricate family portrait. *FEBS Lett* 2012; **586**:2732-2739.
53. Chen MJ, Dixon JE, Manning G. Genomics and evolution of protein phosphatases. *Sci Signal* 2017; **10**:eaag1796.

Figure legends

Figure 1. Workflow for the phosphoproteome analyses of ovarian follicles with or without LH stimulation.

Figure 2. LH-induced NPR2 dephosphorylation in mouse ovarian follicles requires PPP family phosphatase and PKA activities. **(A,B)** The PPP family phosphatase inhibitor cantharidin (51) inhibited LH-induced HA-NPR2 dephosphorylation. Isolated follicles from mice in which endogenous NPR2 was tagged with the HA epitope (16) were treated with or without cantharidin (10 μM, 4 hr) prior to stimulation with 10 nM LH (30 min). Follicle protein was run on a Phos-tag gel and a western blot was probed with an antibody recognizing HA. The decrease in the ratio signal in upper and lower regions of the gel indicated dephosphorylation. Cantharidin inhibited the dephosphorylation. Note that molecular weight markers are not as precise on a Phos-tag gel, and primarily correspond to the least phosphorylated form of a given protein. The graph in B summarizes 3 experiments like that in A. (**C,D**) The PKA inhibitor Rp-8-CPT-cAMPS (34) inhibited LH-induced HA-NPR2 dephosphorylation. Isolated follicles were treated with or without Rp-8-CPT-cAMPS (10 mM, 4 hr) prior to stimulation with 10 nM LH (30 min), and processed as described for A. Rp-8-CPT-cAMPS inhibited the LH-induced dephosphorylation of HA-NPR2. The graph in D summarizes 3 experiments like that in A. (**E,F**) The lower halves of the blots used for C and D were probed with an antibody recognizing phosphorylated CREB (pS133), and the signal was detected with a fluorescent secondary antibody to ensure linearity. The results showed that Rp-8-CPT-cAMPS effectively inhibited PKA. For B, D, and F, each symbol (circle, square, triangle) represents the results from an independently prepared set of samples, each analyzed on a separate blot. Bars show mean ± SEM. Data were analyzed by repeated measures ANOVA followed by the Sidak correction for multiple comparisons.

Figure 3. Quantitative western blot analysis of PPP1R12A phosphosite changes in LH-treated mouse ovarian follicles. Binding of primary antibodies was quantified using a fluorescent secondary antibody and a LI-COR Odyssey imager. (**A**) Representative images of blots of PPP1R12A phosphosites in ovarian follicles treated ± 10 nM LH (30 min). (**B**) Summary of experiments like that in (A). (**C**) PKA-dependence of PPP1R12A-S507 phosphorylation in ovarian follicles. Follicles were treated with or without the PKA inhibitor Rp-8-CPT-cAMPS (10 mM, 8 hr) prior to stimulation with 10 nM LH (30 min). (**D**) Summary of 3 experiments like that in (C), with Rp-8-CPT-cAMPS applied for either 4 or 8 hr. For B and D, each symbol (circle, square, triangle) represents the results from an independently prepared set of samples, each analyzed on a separate blot. Bars show mean ± SEM.

Figure 4. Phostag gel/ western blot analysis of LH-induced phosphosite changes in PPP2R5D in mouse ovarian follicles. Western blots were imaged using a chemiluminescent substrate. (**A**) Standard non-Phostag SDS-PAGE and western blot, showing that PPP2R5D runs as a single band at the expected molecular weight (69 kDa). (**B**) Phos-tag SDS-PAGE and western blot, showing LH-induced PPP2R5D phosphorylation and its PKA-dependence. Follicles were treated with or without the PKA inhibitor Rp-8-CPT-cAMPS (10 mM, 4 hr) then stimulated with 10 nM LH (30 min). Similar results were obtained in 3 other experiments.

Figure 5. No effect of preventing PPP1R12A-S507 phosphorylation on LH-induced NPR2 dephosphorylation. (**A**) Western blot confirming inhibition of LH-stimulated PPP1R12A-S507 phosphorylation in ovarian follicles from *Ppp1r12a*-S507A mice. Similar results were obtained

with 3 sets of samples. (**B**) LH-induced NPR2 dephosphorylation is not inhibited in ovarian follicles from *Ppp1r12a*-S507A mice. (**C**) Summary of 3 experiments like that shown in B. Each symbol (circle, square, triangle) represents the results from an independently prepared set of samples, each analyzed on a separate blot. Bars show mean ± SEM. Data were analyzed by repeated measures two-way ANOVA followed by t-tests with the Holm-Sidak correction. * indicates $p < 0.05$.

Figure 6. No effect of preventing PPP2R5D-S53/S81/S82/S566 phosphorylation on LH-induced NPR2 dephosphorylation in mouse ovarian follicles. (**A**) Western blot confirming inhibition of LH-stimulated PPP2R5D phosphorylation in ovarian follicles from *Ppp2r5d*-4A mice. Similar results were obtained with 3 other sets of samples. (**B**) LH-induced NPR2 dephosphorylation is not inhibited in ovarian follicles from *Ppp2r5d*-4A mice. (**C**) Summary of 4 experiments like that shown in (B). Each symbol (circle, square, triangle, diamond) represents the results from an independently prepared set of samples, each analyzed on a separate blot. Bars show mean ± SEM. Data were analyzed by repeated measures two-way ANOVA followed by t-tests with the Holm-Sidak correction. ** indicates $p < 0.01$.

Figure 1.

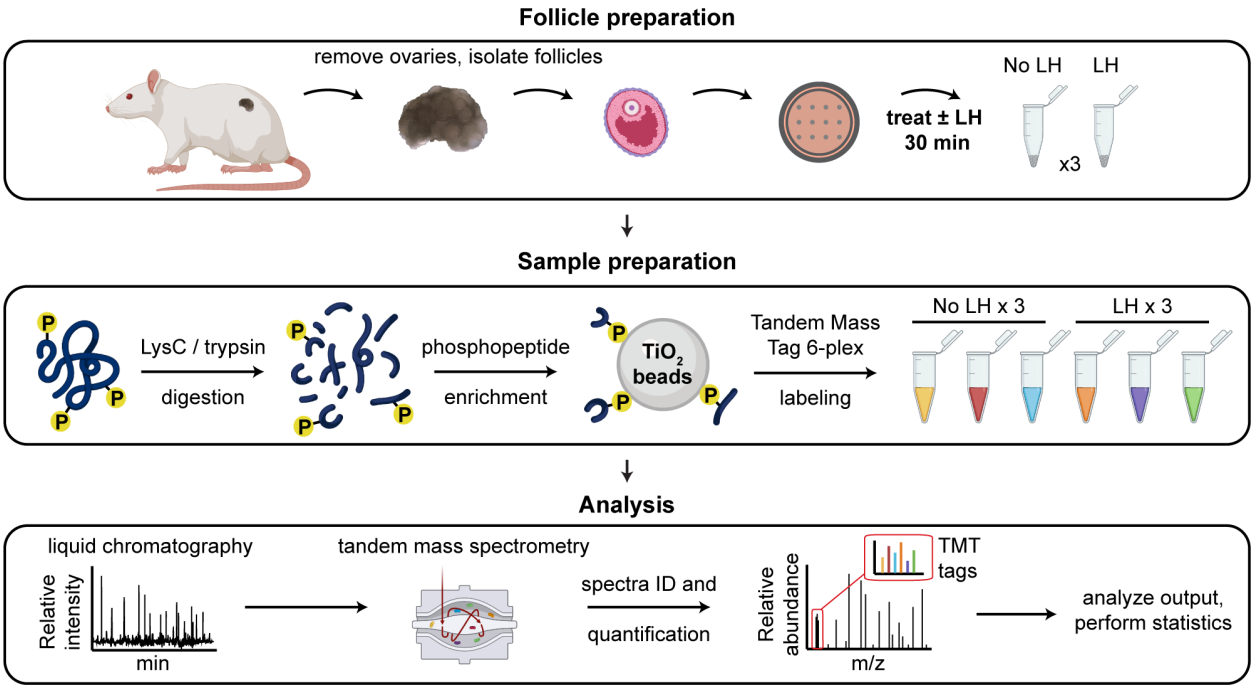
Follicle preparation
remove ovaries, isolate follicles
treat ± LH
30 min
No LH
LH
x3
Sample preparation
LysC / trypsin
digestion
phosphopeptide
enrichment
TiO2
beads
Tandem Mass
Tag 6-plex
labeling
No LH x 3
LH x 3
Analysis
liquid chromatography
Relative
intensity
min
tandem mass spectrometry
spectra ID and
quantification
Relative
abundance
m/z
TMT
tags
analyze output,
perform statistics

Figure 2.

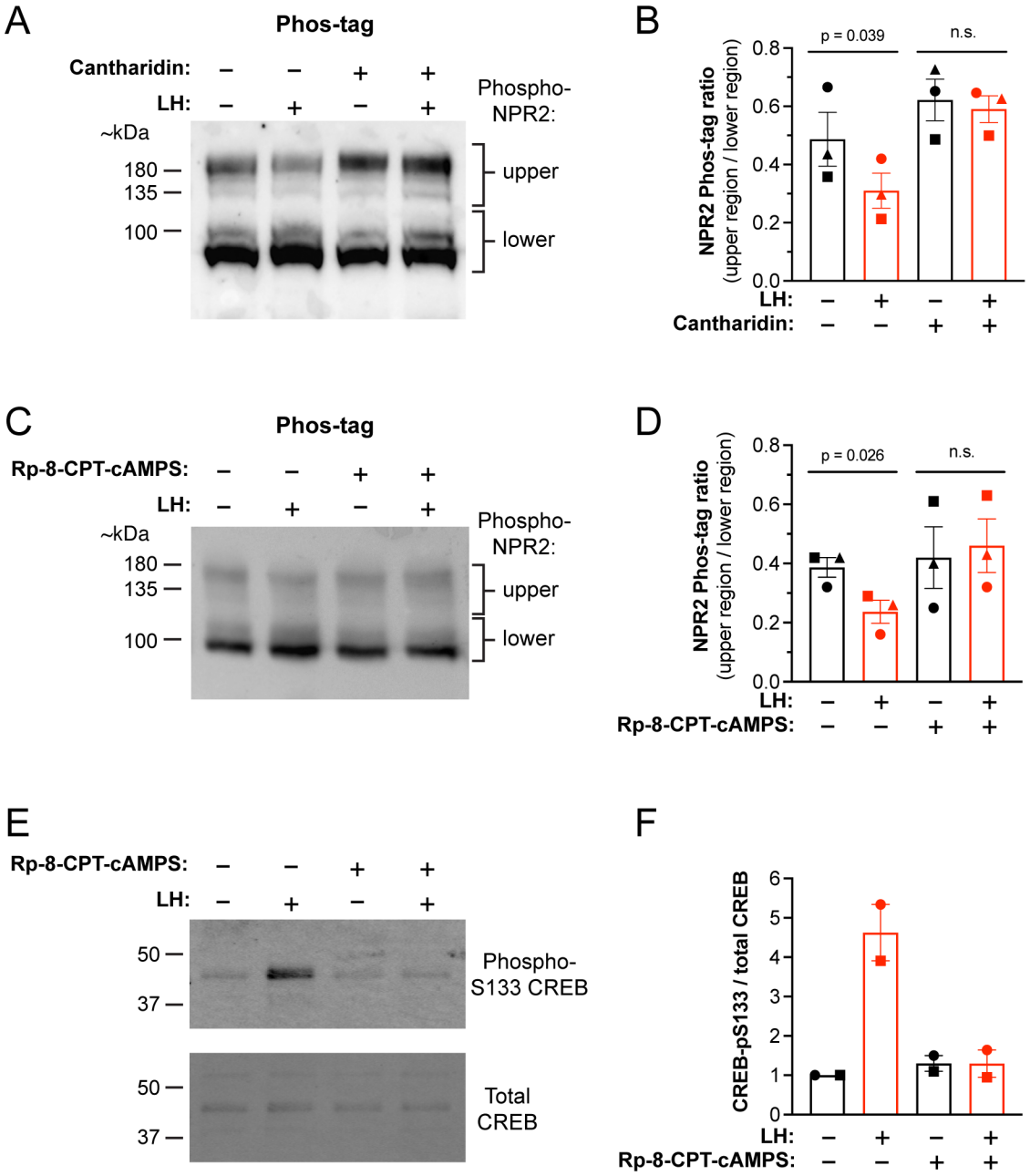
A
Phos-tag
Cantharidin: – – + +
LH: – + – +
~kDa
180
135
100
Phospho-NPR2:
upper
lower
B
p = 0.039
n.s.
NPR2 Phos-tag ratio (upper region / lower region)
0.8
0.6
0.4
0.2
0.0
LH: – + – +
Cantharidin: – – + +
C
Phos-tag
Rp-8-CPT-cAMPS: – – + +
LH: – + – +
~kDa
180
135
100
Phospho-NPR2:
upper
lower
D
p = 0.026
n.s.
NPR2 Phos-tag ratio (upper region / lower region)
0.8
0.6
0.4
0.2
0.0
LH: – + – +
Rp-8-CPT-cAMPS: – – + +
E
Rp-8-CPT-cAMPS: – – + +
LH: – + – +
50
37
Phospho-S133 CREB
50
37
Total CREB
F
CREB-pS133 / total CREB
6
5
4
3
2
1
0
LH: – + – +
Rp-8-CPT-cAMPS: – – + +

Figure 3.

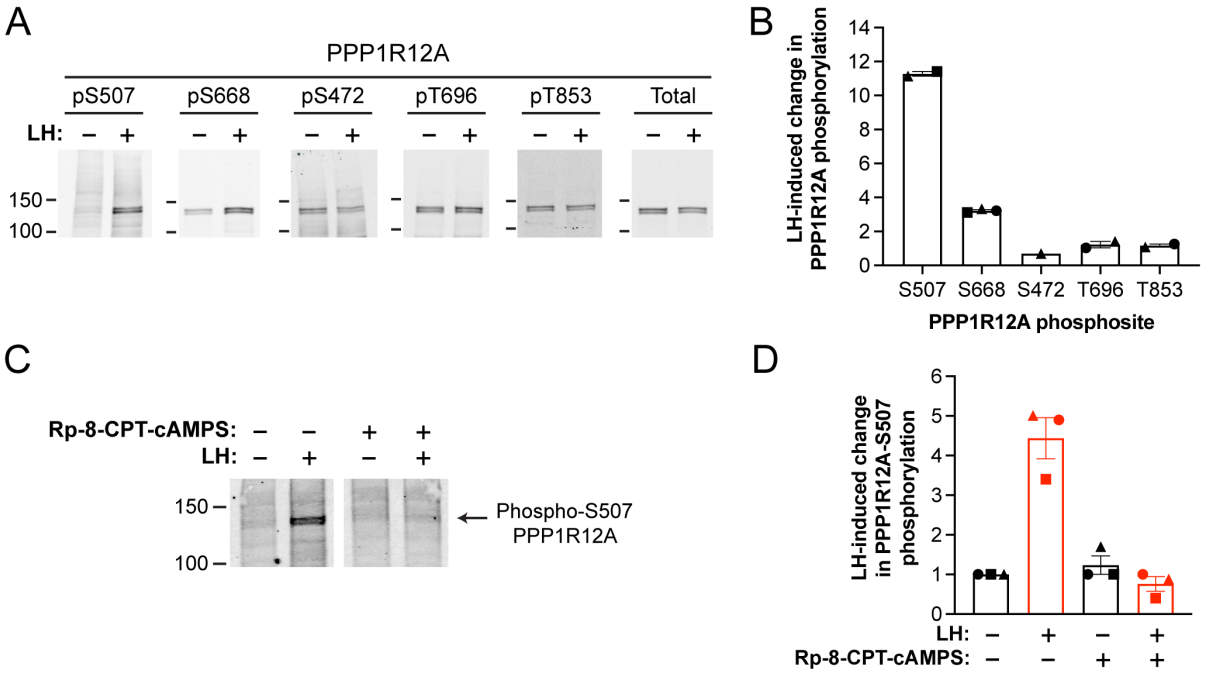
A
PPP1R12A
pS507
pS668
pS472
pT696
pT853
Total
LH:
150
100
B
LH-induced change in PPP1R12A phosphorylation
S507
S668
S472
T696
T853
PPP1R12A phosphosite
C
Rp-8-CPT-cAMPS:
LH:
Phospho-S507 PPP1R12A
D
LH-induced change in PPP1R12A-S507 phosphorylation
LH:
Rp-8-CPT-cAMPS:

Figure 4.

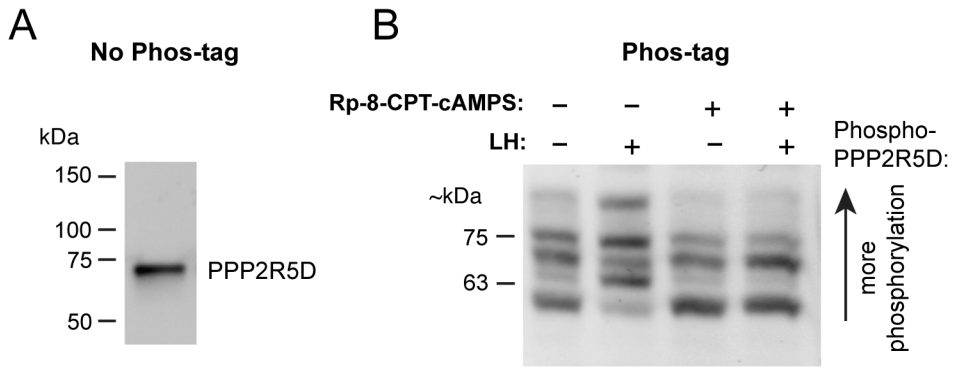
A
No Phos-tag
kDa
150
100
75
50
PPP2R5D
B
Phos-tag
Rp-8-CPT-cAMPS: – – + +
LH: – + – +
Phospho-
PPP2R5D:
~kDa
75
63
more
phosphorylation

Figure 5.

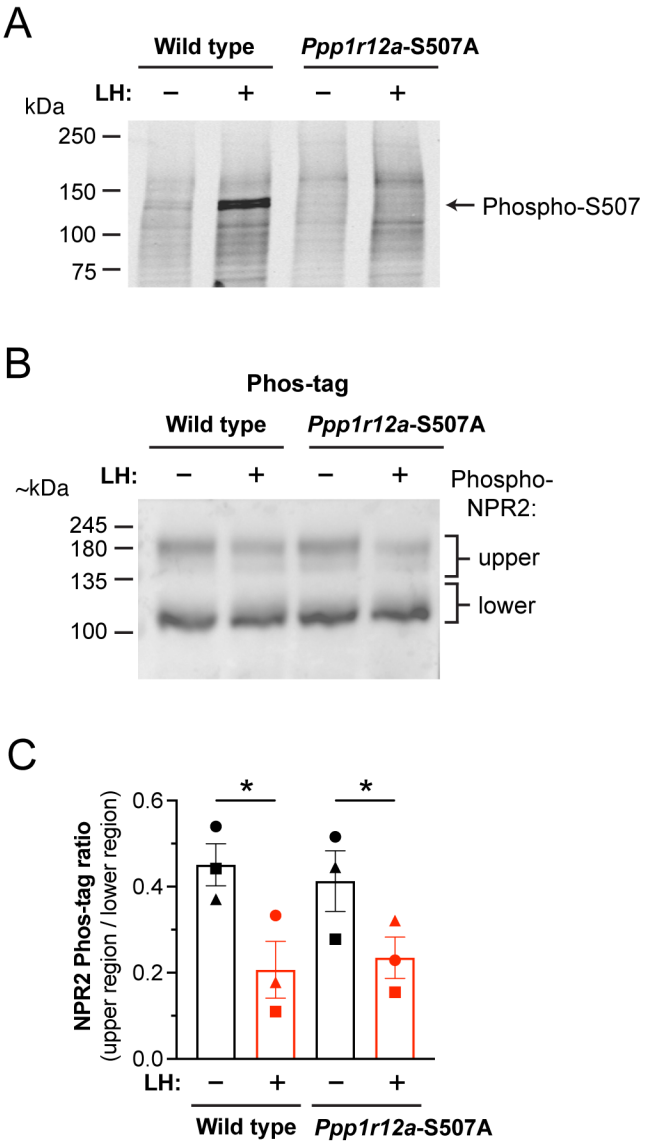
A
Wild type
Ppp1r12a-S507A
LH: − + − +
kDa
250
150
100
75
Phospho-S507
B
Phos-tag
Wild type
Ppp1r12a-S507A
LH: − + − +
~kDa
Phospho-NPR2:
245
180
135
100
upper
lower
C
NPR2 Phos-tag ratio
(upper region / lower region)
0.6
0.4
0.2
0.0
*
*
LH: − + − +
Wild type
Ppp1r12a-S507A

Figure 6.

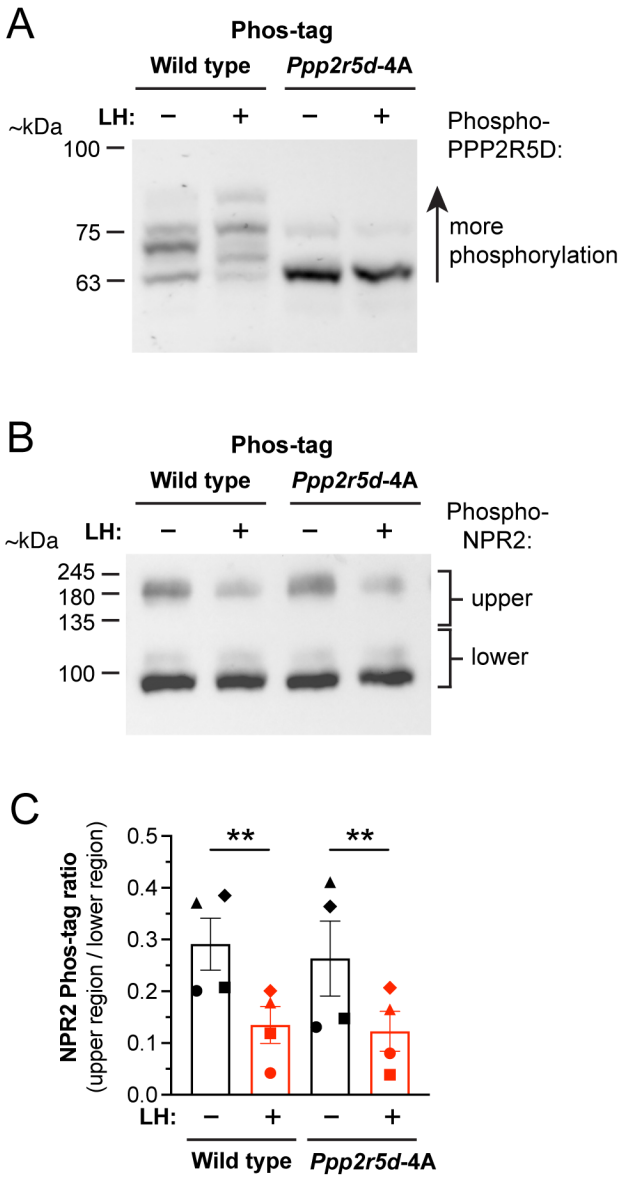
A
Phos-tag
Wild type
Ppp2r5d-4A
~kDa
LH:
−
+
−
+
Phospho-
PPP2R5D:
100
75
63
more
phosphorylation
B
Phos-tag
Wild type
Ppp2r5d-4A
~kDa
LH:
−
+
−
+
Phospho-
NPR2:
245
180
135
100
upper
lower
C
NPR2 Phos-tag ratio
(upper region / lower region)
0.5
0.4
0.3
0.2
0.1
0.0
**
**
LH:
−
+
−
+
Wild type
Ppp2r5d-4A

Table 1. Statistically significant LH-induced changes in phosphopeptide intensity of well-characterized PPP-family phosphatase regulatory subunits in rat ovarian follicles. This list includes all proteins in the Supplementary data file 1 that had official names including "PPP", and for which LH stimulation resulted in a significant change in phosphopeptide intensity. Multiplicity refers to either singly phosphorylated (1) or doubly phosphorylated (2) peptides. Significant increases in phosphopeptide intensity following LH treatment are above the dashed line; significant decreases in phosphopeptide intensity with LH treatment are below the dashed line.

Gene name	UniProt accession	Amino acid	Site #	Multiplicity	Phosphopeptide intensity ($\log_2$ mean ± SEM)		Fold change
					Control	350 nM LH	
PPP2R5D	F1MAA3	S	53	1	16.20 ± 0.03	19.49 ± 0.27	10.4
PPP1R12A*	A0A0G2JWJ0	S	507*	1	16.42 ± 0.06	18.57 ± 0.59	4.7
PPP2R5D	F1MAA3	S	566	1	19.94 ± 0.32	21.90 ± 0.35	4.1
PPP2R5A	D3ZDI7	S	38	1	16.45 ± 0.13	17.92 ± 0.07	2.9
PPP1R9A	O35867	S	185	1	14.20 ± 0.07	15.36 ± 0.14	2.4
PPP2R5C	D4A1A5	S	497	1	19.03 ± 0.18	20.08 ± 0.31	2.2
PPP2R5D	F1MAA3	S	81[#]	2	22.39 ± 0.12	23.15 ± 0.15	1.8
PPP2R5D	F1MAA3	S	82[#]	2	22.12 ± 0.11	22.84 ± 0.17	1.7
PPP1R14A	Q99MC0	S	26	1	22.38 ± 0.02	19.48 ± 0.44	-7.0
PPP1R14A	Q99MC0	S	136	1	18.75 ± 0.24	16.95 ± 0.63	-3.3
PPP1R14A	Q99MC0	S	16	2	17.80 ± 0.05	16.11 ± 0.23	-3.1
PPP1R14A	Q99MC0	S	26	2	17.80 ± 0.05	16.11 ± 0.23	-3.1

* The fragment ion sequence containing this phosphosites is almost identical for PPP1R12A-S507 and PPP1R12B-S502, such that its assignment to PPP1R12A or PPP1R12B is ambiguous. We have assigned it to PPP1R12A because ddPCR analysis showed that PPP1R12A mRNA is present in mouse ovarian follicles at a concentration ~5X higher than PPP1R12B mRNA (Figure S3).

[#] q-values for these sites (0.041 and 0.046, respectively) were just above the significance threshold of 0.01.

Table 2. Statistically significant LH-induced changes in phosphopeptide intensity of non-PPP-family phosphatases in rat ovarian follicles. Previously published lists of phosphatase genes (52, 53) were used to query the phosphopeptide database for significant differences in response to LH. Multiplicity refers to either singly phosphorylated (1) or doubly phosphorylated (2) peptides. Significant increases in phosphopeptide intensity following LH treatment are above the dashed line; significant decreases in phosphopeptide intensity with LH treatment are below the dashed line.

Gene name	UniProt accession	Amino acid	Site #	Multiplicity	Phosphopeptide intensity (log_2 mean ± SEM)		Fold change
					Control	350 nM LH	
CTDSPL2	A0A0G2JTJ5	S	9	1	19.34 ± 0.20	22.47 ± 0.23	9.3
STYXL2/DUSP27	D3ZRM0	S	366	1	14.00 ± 0.36	16.77 ± 0.44	7.2
MTM1	A0A140TAI5	S	23	1	19.09 ± 0.09	21.58 ± 0.34	5.9
SSH1	F1LWM1	S	576	1	17.94 ± 0.22	19.79 ± 0.51	3.8
CTDSPL2	A0A0G2JTJ5	S	28	1	20.59 ± 0.38	22.35 ± 0.53	3.6
SSH1	F1LWM1	S	598	1	17.32 ± 0.08	19.04 ± 0.48	3.5
SGPP1	Q99P55	S	96	2	18.13 ± 0.02	19.72 ± 0.33	3.2
SGPP1	Q99P55	S	101	2	18.13 ± 0.02	19.72 ± 0.33	3.2
PPIP5K2	A0A096MK18	S	593	1	15.81 ± 0.27	16.96 ± 0.37	2.3
MTMR2	D3ZA31	S	58	1	19.38 ± 0.24	15.13 ± 1.38	-17.9
PPM1H	Q5M821	T	113	1	18.58 ± 0.39	15.47 ± 0.86	-8.1
MTMR6	A0A0G2JXT6	S	623	1	18.49 ± 0.12	16.42 ± 0.69	-3.9
PTPN21	A0A0G2JTB7	S	728	1	16.57 ± 0.14	14.64 ± 0.72	-3.6
STYXL2/DUSP27	D3ZRM0	S	1015	1	18.26 ± 0.17	16.41 ± 0.05	-3.4
MTMR9	Q5XIN4	S	548	1	20.42 ± 0.19	18.80 ± 0.60	-2.9
SYNJ1	Q62910	T	1217	1	21.09 ± 0.03	19.57 ± 0.40	-2.7
MTMR12	Q5FVM6	S	602	1	17.86 ± 0.09	16.52 ± 0.43	-2.4
STYXL2/DUSP27	D3ZRM0	S	1015	1	16.50 ± 0.09	15.27 ± 0.32	-2.2

SUPPLEMENTARY MATERIAL

Identification of protein phosphatases modified by luteinizing hormone signaling in ovarian follicles

Jeremy R. Egbert, Ivan Silbern, Tracy F. Uliasz, Katie M. Lowther, Siu-Pok Yee, Henning Urlaub, and Laurinda A. Jaffe

Figure S1. Generation of *Ppp1r12a*-S507A mice.

Figure S2. Generation of *Ppp2r5d*-S53A/S81A/S82A/S566A mice

Figure S3. PPP1R12A mRNA is ~5 times more abundant than PPP1R12B mRNA in mouse ovarian follicles.

Figure S4. Statistically significant LH-induced phosphorylation changes in cofilin/actin depolymerizing factor family proteins CFL1, CFL2, and DSTN, and in the Slingshot phosphatase SSH1 that dephosphorylates these proteins.

Table S1. Antibodies used for western blotting.

Table S2. Statistically significant LH-induced changes in phosphopeptide intensity of proteins in rat ovarian follicles that have been reported to form complexes with PPP family phosphatase catalytic subunits, other than those listed in Table 1.

Supplementary Data File 1. Full table of phosphorylation changes in rat follicles ± LH (Excel)

Supplementary Data File 2. Full table of quantified protein intensities in rat follicles ± LH (Excel)

Supplementary Data File 3. Full list of plots visualizing phosphorylation changes in rat follicles (PDF)

Supplementary Data File 4. Gene Ontology—Biological Process enrichment analysis of rat follicle proteins that are significantly differentially phosphorylated in response to LH (Excel)

Supplementary Data File 5. Gene Ontology—Cellular Compartment enrichment analysis of rat follicle proteins that are significantly differentially phosphorylated in response to LH (Excel)

Supplementary Data File 6. Gene Ontology—Molecular Function enrichment analysis of rat follicle proteins that are significantly differentially phosphorylated in response to LH (Excel)

Figure S1. Generation of *Ppp1r12a*-S507A mice. To introduce the S507A mutation into *Ppp1r12a* (indicated in bold pink type), we employed CRISPOR (http://crispor.tefor.net) and identified a CRISPR cleavage site (5'- CTC TTC AAT GTC AGA TGT AC) adjacent to S507 in exon 11 of *Ppp1r12a*. The PAM sequence is underlined. CRISPR/Cas9 ribonucleoprotein together with single-strand DNA donor were electroporated into one-cell embryos from C57BL/6J mice that had been previously modified to insert an HA tag on the N-terminus of *Npr2* (16). The embryos were then transferred into foster females for subsequent development. PCR genotyping was performed to screen for potential founders using the primer pair PS507AF and P1r12a I12R, which amplifies a fragment of 135 bp specific to the S507A knockin mutation. Founders were further confirmed by PCR using primer pair P1r12a I11F and P1r12a I12R to amplify a fragment of 258 bp containing the S507A mutation followed by sequencing of the PCR product. Founders were then bred with C57BL/6J mice (with HA-tagged *Npr2*) to establish the *Ppp1r12a*-S507A mouse line.

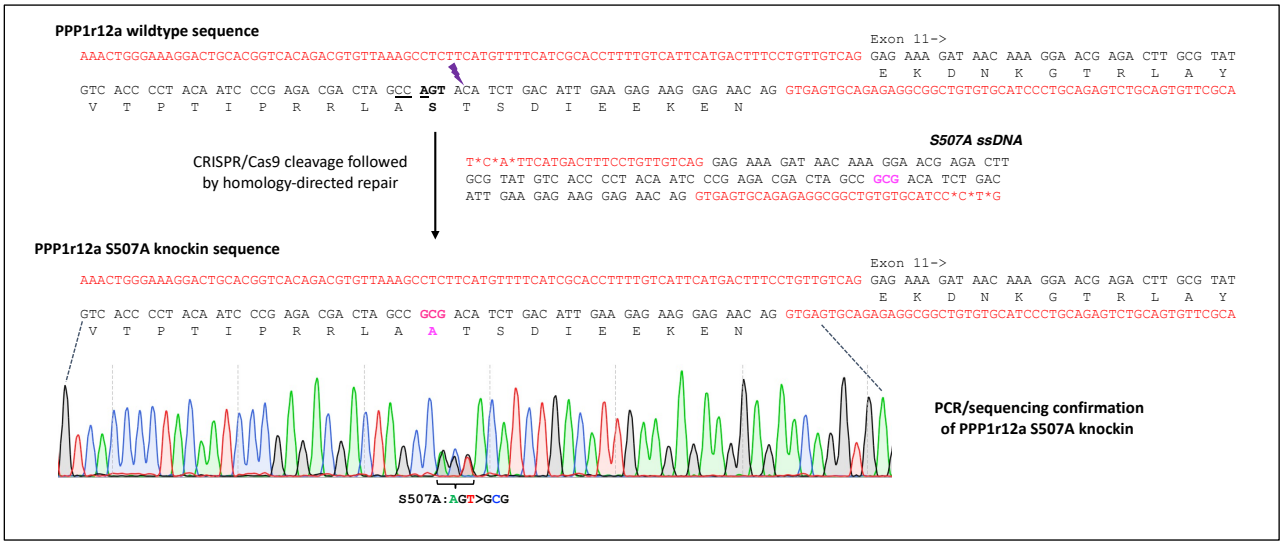

DNA sequences for generation and genotyping of PPP1R12A-S507A mice.

(* represents phosphorothioate linkages to prevent degradation from exonuclease)

Type of sequence	Sequence
sgRNA	5'- CTCTTCAATGTCAGATGTAC
S507A ssDNA donor (sense)	5'- T*C*A*TTCATGACTTTCCTGTTGTCAG GAG AAA GAT AAC AAA GGA ACG AGA CTT GCG TAT GTC ACC CCT ACA ATC CCG AGA CGA CTA GCC **GCG** ACA TCT GAC ATT GAA GAG AAG GAG AAC AG_GTGAGTGCAGAGAGGCGGCTGTGTGCATCC*C*T*G
PS507AF (Forward genotyping primer)	5'- CAATCCCGAGACGACTAGCCGCG

P1r12a I12R (Reverse genotyping primer)	5’- GCTCGCATCAGTCCTCACATC
P1r12a I11F (PCR/sequencing)	5'- GACTGCACGGTCACAGACGTG
P1r12a I12R (PCR/sequencing)	5'- GCTCGCATCAGTCCTCACATC

Figure S2. Generation of *Ppp2r5d*-S53A/S81A/S82A/S566A mice, nicknamed *Ppp2r5d*-4A. These mice were generated in a two-step process. *Ppp2r5d*-S566A mice were generated first, then bred to homozygosity to provide embryos for generation of the final *Ppp2r5d*-4A mice. (**A**) We identified a CRISPR site cleavage site (5'- GAG GAA GTC AGA GCT GCC AC) close to S566 in exon 15 using CRISPOR (http://crispor.tefor.net). The PAM site is underlined. A G>A silent mutation in Q560 was included in the S566A ssDNA donor to eliminate the PAM in order to prevent re-cleavage of the S566A knockin allele. S566A ssDNA and CRISPR/Cas9 ribonucleoprotein were electroporated into one-cell embryos from C57BL/6J mice that had been previously modified to insert an HA tag on the N-terminus of *Npr2* (16). The embryos were then transferred into a foster mother for subsequent development. Founder pups were identified by PCR genotyping using the primer pair PS566AF and PppE15R1, to amplify a 157 bp fragment specific to the S566A knockin. Their genotypes were confirmed by PCR using primer pair Ppp I14F1 and Ppp E15R1 to amplify a fragment of 255 bp containing the S566A knockin mutation followed by sequencing of the PCR product. (**B**) Two CRISPR sites adjacent to S53 (sgRNA1) and S81/S82 (sgRNA2) were identified. CRISPR/Cas9 ribonucleoproteins and 3A ssDNA were electroporated into homozygous *Ppp2r5d*-S566A one-cell embryos. Founders containing the S53A/S81A/S82A knockin mutations were identified using the primer pair S53.E3F1 and S81.82E3R1 to specifically amplify a fragment of 120 bp, and their identities were further confirmed by PCR using primer pair P2r5d.SeqF and P2r5d.SeqR to amplify a fragment of 383 bp containing the S53A/S81A/S82A mutations followed by sequencing of the PCR product. Founders were bred with C57BL/6J mice (with HA-tagged *Npr2*) to establish the *Ppp2r5d*-4A mouse line.

A

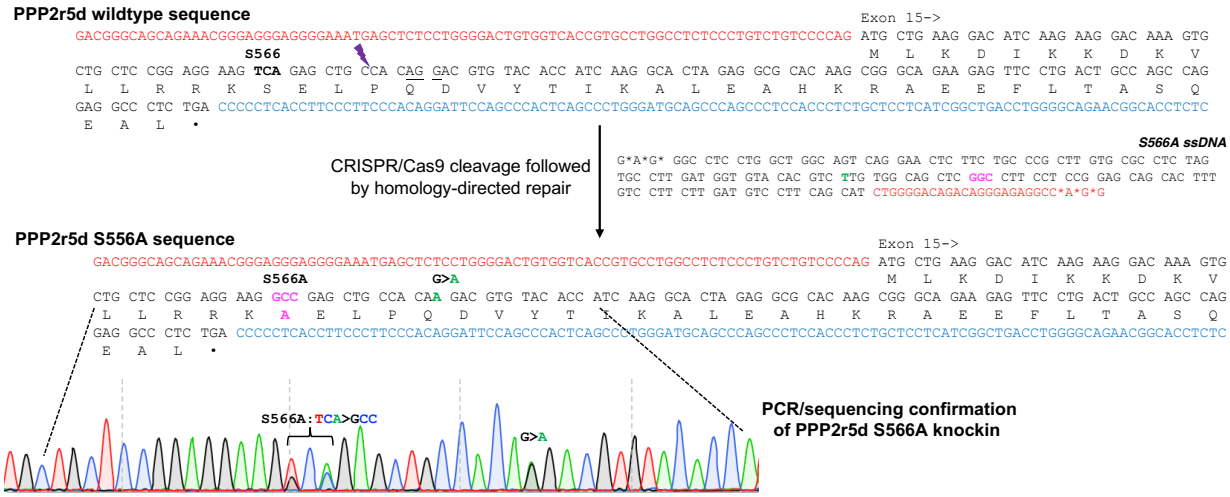

DNA sequences for generation and genotyping of PPP2R5D-S566A mice.

(* represents phosphorothioate linkages to prevent degradation from exonuclease)

Type of sequence	Sequence

sgRNA	5'- GAGGAAGTCAGAGCTGCCAC
S566A ssDNA donor (antisense)	5'- G*A*G*GGCCTCCTGGCTGGCAGTCAGGAACTCTTCTGCCCGCTTG TGCGCCTCTAGTGCCTTGATGGTGTACACGTCTTGTGGCAGCTCG GCCTTCCTCCGGAGCAGCACTTTGTCCTTCTTGATGTCCTTCAGCA TCTGGGGACAGACAGGGAGAGGCC*A*G*G
PppS566AF (Forward genotyping primer)	5'- AAGTGCTGCTCCGGAGGAAGGCC
PppE15R1 (Reverse genotyping primer)	5'- GGGCTGAGTGGGCTGGAATCC
Ppp I14F1 (PCR/sequencing)	5' - ACGGGAGGGAGGGGAAATGAGC
Ppp E15R1 (PCR/sequencing)	5' - GGGCTGAGTGGGCTGGAATCC

B

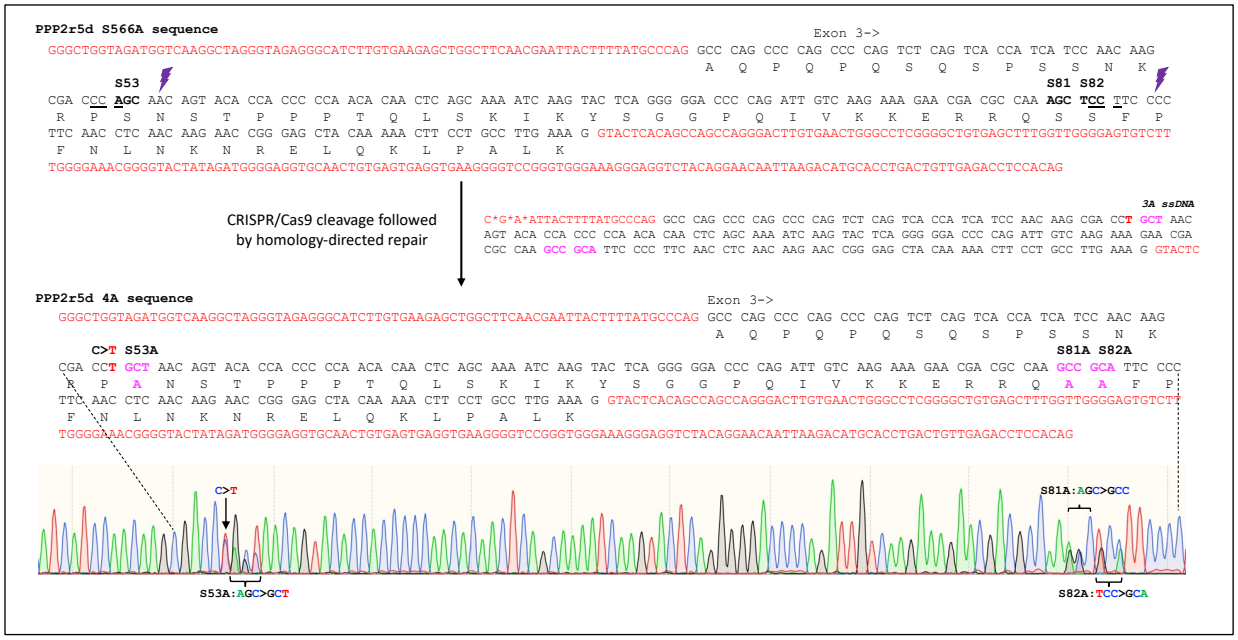

DNA sequences for generation and genotyping of PPP2R5D-4A mice.

(* represents phosphorothioate linkages to prevent degradation from exonuclease)

Type of sequence	Sequence
sgRNA1	5'- TGGGGGTGGTGTACTGTTGC
sgRNA2	5'- CTTGTTGAGGTTGAAGGGGA
3A ssDNA donor (sense)	5'- C*G*A*ATTACTTTTATGCCCAGGCCCAGCCCCAGCCCCAGTCTCAG TCACCATCATCCAACAAGCGACCTGCTAACAGTACACCACCCCCAA CACAACTCAGCAAAATCAAGTACTCAGGGGGACCCCAGATTGTCAA GAAAGAACGACGCCAAGCCGCATTCCCCTTCAACCTCAACAAGAA CCGGGAGCTACAA AAACTTCCTGCCTTGAAAGGTACTC
S53.E3F1 (Forward genotyping primer)	5'- CATCCAACAAGCGACCTGCT
S81.82E3R1 (Reverse genotyping primer)	5'- GAGGTTGAAGGGGAATGCGGC
P2r5d.SeqR (PCR/sequencing)	5' - GAGGGCTGGTAGATGGTCAAG
P2r5d.SeqR (PCR/sequencing)	5' - CTCACAGTTGCACCTCCCCAT

Figure S3. PPP1R12A mRNA is ~5 times more abundant than PPP1R12B mRNA in mouse ovarian follicles. The bars show the mean ± SEM for analysis of 3 independent preparations of RNA.

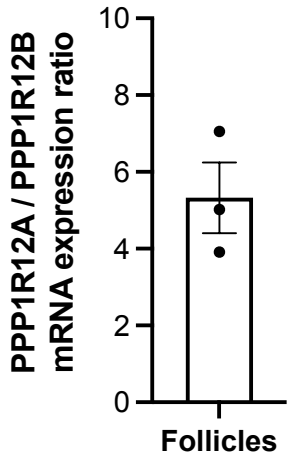

Methods: RNA from mouse preovulatory follicles was extracted with Trizol and treated with DNAse. ddPCR was performed using a Bio-Rad QX-200 Droplet Digital system and primers as listed below. We thank Andrew Collins and Angela Ross (Bio-Rad) for performing the ddPCR assay.

Primer sequences used for ddPCR to compare amounts of PPP1R12A and PPP2R12B mRNA.

Gene name	Forward	Reverse	Amplicon
Ppp1r12a	5'-CTCTATGCCTCAAGTCAGCTC	5'-GCTGTGACTTATCTTCCCCTTC	139 bp
Ppp1r12b	5'-AGAAGCTTGAAGATCCTGGTG	5'-TGGGTTTGTCTGGTTGAGTTG	150 bp

Figure S4. Statistically significant LH-induced phosphorylation changes the Slingshot phosphatase SSH1 and in cofilin/actin depolymerizing factor family proteins CFL1, CFL2, and DSTN that are dephosphorylated by SH1. SSH1 showed ~4x increases in phosphorylation intensity at S576 and S598. CFL1, CFL2, and DSTN all showed a decrease in phosphorylation intensity of serine 3; dephosphorylation at this conserved site activates actin-depolymerizing activity of these proteins (44). LH-induced changes in phosphorylation intensity of other sites of CFL1, CFL2, and DSTN were also detected.

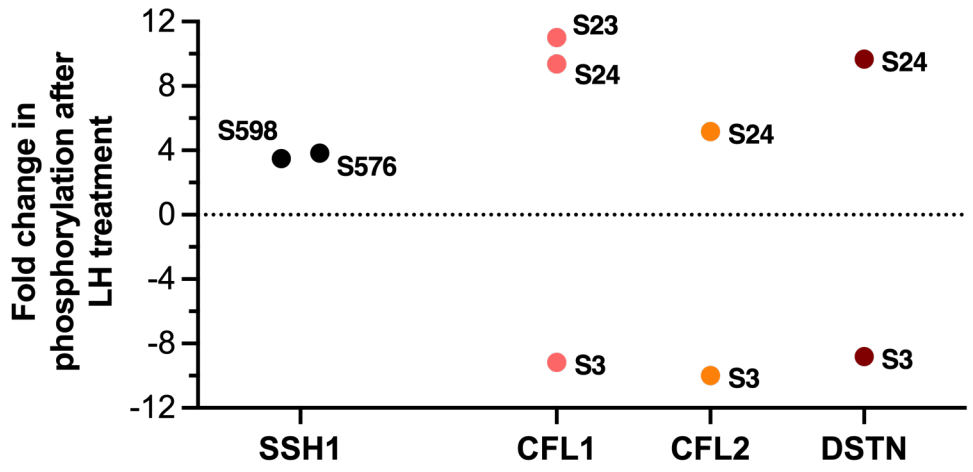

Table S1. Antibodies used for western blotting

Target	Supplier	Catalog #	Dilution	RRID
HA epitope tag (6E2)	Cell Signaling Technology	2367	1:1000	AB_10691311
Phospho-S133 CREB	EMD Millipore	05-667	1:500	AB_309889
Total CREB	Cell Signaling Technology	9197	1:1000	AB_331277
Phospho-S507 PPP1R12A (P-MYPT1)[a]	Cell Signaling Technology	3040	1:1000	AB_2168424
Phospho-S668 PPP1R12A (P-MYPT1)	Cell Signaling Technology	3048	1:1000	AB_2168418
Phospho-S472 PPP1R12A (P-MYPT1)	Invitrogen	PA5-114608	1:1000	AB_2899244
Phospho-T696 PPP1R12A (P-MYPT1)	Cell Signaling Technology	5163	1:1000	AB_10691830
Phospho-T853 PPP1R12A (P-MYPT1)	Cell Signaling Technology	4563	1:1000	AB_1031185
Total PPP1R12A (MYPT1)	Cell Signaling Technology	2634	1:1000	AB_915965
Total PPP2R5D	Abcam	ab188323	1:10000	--
IRDye® 800CW Goat anti-Rabbit IgG Secondary Antibody	LI-COR	925-32211	1:15000	AB_10956166
IRDye® 680RD Goat anti-Rabbit IgG Secondary Antibody	LI-COR	926-68071	1:15000	AB_621842
IRDye® 800CW Goat anti-Mouse IgG Secondary Antibody	LI-COR	926-32210	1:15000	AB_10718209
Goat-anti-mouse IgG (H+L), HRP conjugate	Advansta	R-05071-500	1:20000	--

[a]The antigen used to make this antibody is 100% identical to the mouse PPP1R12A sequence, and 85% identical to the mouse PPP1R12B sequence. Therefore, this antibody would also recognize Phospho-S502 of PPP1R12B.

Table S2. Statistically significant LH-induced changes in phosphopeptide intensity of proteins in rat ovarian follicles that have been reported to form complexes with PPP family phosphatase catalytic subunits, other than those listed in Table 1. Previously published lists of validated PPP family-interacting proteins (14,15) were used to query the phosphopeptide database for significant differences in response to LH. Multiplicity refers to either singly phosphorylated (1) or doubly phosphorylated (2) peptides. Significant increases in phosphopeptide intensity following LH treatment are above the dashed line; significant decreases in phosphopeptide intensity with LH treatment are below the dashed line.

Gene name	UniProt accession	Amino acid	Site #	Multiplicity	Phosphopeptide intensity (log_2 mean ± SEM) Control	350 nM LH	Fold change
HDAC6*	A0A0G2QC41	S	59	1	14.56 ± 0.61	18.64 ± 1.07	18.0
STRN3*	E9PT82	S	239	2	15.24 ± 0.08	19.02 ± 0.18	14.6
STRN3*	E9PT82	S	255	2	15.24 ± 0.08	19.02 ± 0.18	14.6
PLCL1	F1LP62	S	19	2	17.04 ± 0.13	20.14 ± 0.06	9.1
EIF2AK2	M0RDJ3	S	212	1	18.95 ± 0.18	21.94 ± 0.26	8.5
FARP1*	F1LYQ8	S	513	2	13.80 ± 0.21	16.70 ± 0.18	7.9
FARP1*	F1LYQ8	S	517	2	13.80 ± 0.21	16.70 ± 0.18	7.9
MAP1B*	P15205	S	561	1	22.90 ± 0.12	25.52 ± 0.31	6.5
ZFYVE16	D4ADF6	S	903	2	17.57 ± 0.24	20.17 ± 0.09	6.5
ZFYVE16	D4ADF6	S	907	2	17.57 ± 0.24	20.17 ± 0.09	6.5
PHACTR4*	M0R7T1	S	159	2	18.97 ± 0.16	21.52 ± 0.12	6.2
APC*	G3V8Q9	S	2793	1	18.43 ± 0.11	20.87 ± 0.19	5.8
MKI67	D4A0Y6	S	124	1	17.98 ± 0.02	20.41 ± 0.24	5.7
PHACTR4*	M0R7T1	S	162	2	19.29 ± 0.20	21.68 ± 0.13	5.5
AKAP1	D4A9M6	S	425	1	17.01 ± 0.06	29.39 ± 0.11	5.5
APC*	G3V8Q9	S	2817	2	15.38 ± 0.33	17.67 ± 0.21	5.2
APC*	G3V8Q9	S	2829	2	15.67 ± 0.27	17.77 ± 0.18	4.6
APC*	G3V8Q9	T	2819	2	14.37 ± 0.25	16.23 ± 0.10	3.8
PLCL1	F1LP62	T	15	2	19.78 ± 0.11	21.58 ± 0.07	3.7
SH2D4A	Q6AYC8	S	51	1	18.21 ± 0.21	20.01 ± 0.39	3.7
PCIF1	D4A417	T	135	3	14.49 ± 0.25	16.29 ± 0.14	3.7
SLC9A1	P26431	S	707	2	19.21 ± 0.14	20.98 ± 0.09	3.6
AKAP11	A0A0G2JZI9	S	21	1	17.30 ± 0.37	19.05 ± 0.37	3.6
PLCL1	F1LP62	S	491	1	11.53 ± 0.35	13.23 ± 0.24	3.4
PCIF1	D4A417	T	150	2	18.36 ± 0.37	20.05 ± 0.09	3.4
PCIF1	D4A417	T	135	2	16.05 ± 0.44	17.73 ± 0.28	3.4
PCIF1	D4A417	S	140	3	16.06 ± 0.23	17.66 ± 0.16	3.2
PLCL1	F1LP62	S	17	2	19.58 ± 0.13	21.12 ± 0.07	3.1
SLC9A1	P26431	S	697	2	20.56 ± 0.11	22.09 ± 0.14	3.1
SLC9A1	P26431	S	776	2	16.38 ± 0.10	17.86 ± 0.17	3.0
MAP1B*	P15205	S	985	2	23.10 ± 0.09	24.56 ± 0.16	2.9
MAP1B*	P15205	S	988	2	23.10 ± 0.09	24.56 ± 0.16	2.9
MAP1B*	P15205	S	1454	2	17.42 ± 0.41	18.86 ± 0.14	2.9
MAP1B*	P15205	S	1465	2	17.42 ± 0.41	18.86 ± 0.14	2.9
MAP1B*	P15205	T	1262	3	19.12 ± 0.26	20.51 ± 0.06	2.8
SLC9A1	P26431	S	606	2	17.61 ± 0.02	19.00 ± 0.15	2.8
MKI67	D4A0Y6	S	336	1	19.80 ± 0.08	21.09 ± 0.22	2.6
SLC9A1	P26431	S	790	2	19.02 ± 0.07	20.22 ± 0.12	2.4
SET*	Q63945	S	28	2	18.89 ± 0.06	20.09 ± 0.11	2.4

SET*	Q63945	S	30	2	18.89 ± 0.06	20.09 ± 0.11	2.4
MAP1B*	P15205	S	1471	1	17.76 ± 0.11	18.90 ± 0.32	2.3
CASP9	Q9JHK1	S	348	2	14.65 ± 0.09	15.70 ± 0.26	2.2
CASP9	Q9JHK1	S	350	2	14.65 ± 0.09	15.70 ± 0.26	2.2
AKAP1	D4A9M6	S	101	1	18.57 ± 0.07	19.60 ± 0.31	2.2
HDAC6*	A0A0G2QC41	S	43	1	22.25 ± 0.11	19.52 ± 0.37	-6.2
HDAC6*	A0A0G2QC41	S	859	1	21.50 ± 0.12	19.27 ± 0.61	-4.4
MAP1B*	P15205	T	527	1	21.25 ± 0.23	19.10 ± 0.73	-4.2
AKAP1	D4A9M6	S	103	1	19.38 ± 0.19	17.48 ± 0.51	-3.5
PHACTR2*	A0A0G2K8Q4	T	22	1	20.29 ± 0.23	18.48 ± 0.73	-3.3
FARP1*	F1LYQ8	S	427	2	20.51 ± 0.31	18.85 ± 0.13	-3.0
FARP1*	F1LYQ8	S	435	2	20.51 ± 0.31	18.85 ± 0.13	-3.0
PHACTR2*	A0A0G2K8Q4	S	154	1	18.30 ± 0.08	16.65 ± 0.40	-3.0
MAP1B*	P15205	S	541	1	24.80 ± 0.03	23.33 ± 0.40	-2.6
APC*	G3V8Q9	S	2556	2	17.80 ± 0.18	16.35 ± 0.19	-2.6
MAP1B*	P15205	T	1959	1	17.86 ± 0.12	16.45 ± 0.35	-2.5
SLC9A1	P26431	S	790	1	22.26 ± 0.11	20.91 ± 0.47	-2.4
APC*	G3V8Q9	S	2556	2	19.43 ± 0.08	18.22 ± 0.36	-2.2

* Proteins known to regulate the cytoskeleton and/or cell motility according to the National Center for Biotechnology Information (NCBI) gene summaries.